Wear reduction mechanism in modulated turning of nodular graphite iron with coated carbide tool

Aaqib Ali[a], Patrick Kwon[a] and Yang Guo[a,*]

[a]Department of Mechanical Engineering, Michigan State University, East Lansing, 48824, MI, USA

ARTICLE INFO

Keywords:
modulation-assisted machining
nodular graphite iron
ductile cast iron
tool wear
tool protective layer

ABSTRACT

Modulation-assisted machining (MAM) is used for turning nodular graphite iron (NGI) with coated carbide tools and compared with conventional machining (CM) at the cutting speed of 350 m/min in dry and wet conditions. Significant reductions in flank wear are achieved using MAM as compared to CM turning, in both dry and wet conditions. Dry MAM results in even lower wear than wet MAM condition. The substantial wear reduction in dry MAM is due to the formation of two material layers (i.e., the MgO deposition layer and the stagnated iron layer) and their unique arrangement on the flank face of the tool. The protective effect of these layers and the MAM conditions conducive to the formation of these layers are discussed.

1. Introduction

Due to its distinct graphite morphology in the iron matrix, nodular graphite iron (NGI), also called spheroidal graphite iron, ductile cast iron, or nodular cast iron, has both higher strength and toughness than the most common flake graphite iron (FGI), i.e., gray cast iron. The elastic modulus of NGI is also higher than that of FGI. Therefore, NGI has a wide range of applications, in general, for parts requiring higher fatigue resistance and elastic modulus, such as rolling mill rolls, automotive crankshafts, gears, bearing caps, clutch housings, axle carriers, and wind turbine hubs [1, 2]. However, NGI is more difficult to machine than FGI. For identical cutting conditions, tool life is significantly shorter in cutting NGI than FGI, especially at high cutting speeds (>200 m/s). This again can be attributed to the higher strength and toughness of NGI. The spheroidal graphite greatly improves the fracture toughness of the iron as compared to the flake graphite, so chip formation in NGI is associated with extensive plastic deformation, more heat generation, and higher cutting temperature, which leads to higher tool wear [3]. As a result, NGI is usually machined at much lower speeds compared to FGI [2].

Earlier studies on the machinability of NGI mainly focused on the performance evaluation of various cutting tool materials and coatings for machining NGI. Yigit et al. [4] investigated the performance of uncoated and multi-layer (TiCN + TiC + TiCN + Al_2O_3 + TiN) coated carbide tools in turning NGI at speeds ranging from 125 to 200 m/min. Their results showed that although coated carbide tools performed better than uncoated carbide tools, the tool life decreased significantly with increasing the cutting speed. At the speed of 200 m/min, the coated carbide tool reached the end of tool life (flank wear land of 300 µm) at a cutting distance of ≈ 350 m. Tooptong et al. [5] investigated the performance of uncoated and multi-layer (TiCN + Al_2O_3 + TiN) coated carbide tools in turning three cast irons including FGI, compacted graphite iron (CGI), and NGI at three speeds (150, 250 and 350 m/min). Their results showed that cutting CGI and NGI led to comparable tool wear, which was significantly higher than cutting FGI, especially at the higher cutting speeds (250 and 350 m/min). For cutting NGI at 350 m/min, although the coated carbide tool performed better than the uncoated carbide tool, the end of tool life was reached (flank wear land of 300 µm) at a cutting distance of ≈ 1800 m. Grzesik and Matecka [6] investigated the performance of uncoated and Al_2O_3 /TiN coated Si_3N_4 ceramic tools in turning NGI at the cutting speeds of 100, 160, and 240 m/min. Their results showed the coated ceramic tools performed better than the uncoated ceramic tools. At the cutting speed of 240 m/min, the coated ceramic tool reached its tool life at a cutting distance of ≈ 500 m. Camuscu [7] investigated the performance of Al_2O_3 based ceramic tools in turning NGI at the cutting speed ranging from 300 to 750 m/min. The TiN coated Al_2O_3 +TiCN mixed ceramic tool showed better performance than the other tested tools. Extrapolated from the wear curves, the tool life was reached (flank wear land of 300 µm) at a cutting distance of ≈ 2000 m and ≈ 1000 m when the cutting speed was 300 m/min

*Corresponding author
yguo@msu.edu (Y. Guo)
ORCID(s):

Table 1
Chemical composition of the NGI work material.

Elements	Carbon (C)	Silicon (Si)	Manganese (Mn)	Phosphorus (P)	Sulfur (S)
Percentage	3.7	2.63	0.25	0.05	0.025

and 750 m/min, respectively. Grzesik et al. [8] investigated the performance of CBN tool in turning NGI at cutting speeds ranging from 100 to 480 m/min. Based on their results, the recommended cutting speed range was 240 - 320 m/min for the CBN tools. At the speed of 320 m/min, the tool life was reached (flank wear land of 300 μm) at a cutting distance of ≈ 2400 m.

From the above survey, although various cutting tools (carbide, ceramic, CBN) and their coating materials have been tested, there has not been any standout tool material and coating that can drastically improve the wear performance for machining NGI at speeds > 250 m/min. For example, based on the above survey, the best tool life for respective carbide, ceramic, and CBN tools is at around 2000 m cutting distance at the speed level of ≈ 300 m/min [5][7][8]. Therefore, the current cutting tool and coating technology alone may not be enough to improve the poor machinability of NGI. Nayyar et al. concluded from their study [9] that coolant needs to be applied when machining NGI at high cutting speeds, especially in continuous cutting operations such as turning, boring, and drilling. However, the cooling effect is largely dependent on the abundance of applied coolant which can incur significant material and waste handling costs [10].

Modulation-assisted machining (MAM) is a novel machining technique that utilizes controlled low-frequency (tens or hundreds of Hz) tool vibration in the feed direction to enhance the cutting process [11]. The applied feed modulation transforms a continuous cutting process (i.e., turning, boring, or drilling) into a discrete cutting process, leading to benefits including robust chip breaking, periodic tool-chip contact disruption, better coolant action, and hence, reduced thermomechanical loads on the cutting tool. It has been shown that MAM can drastically enhance the tool life for turning compacted graphite iron (CGI). When turning CGI with CBN tool in wet condition at the speed range of 550 – 730 m/min, tool life can be increased at least 20x in MAM compared to conventional machining (CM) [12]. When turning CGI with coated carbide tools in dry condition at the speed range of 250 – 350 m/min, tool life can also be increased multiple times in MAM compared to CM [13]. More interestingly, turning CGI with a coated carbide tool in dry condition results in better wear performance than in wet condition. This has been explained by the formation of the SiO_2 deposition layer and stagnated iron layer on the flank face which protects the tool during cutting and which only occurs in MAM dry cutting condition [14].

Since MAM can drastically reduce tool wear in cutting CGI and similar poor machinability exists with NGI, it is reasonable to expect that MAM can also effectively enhance the machinability of NGI. However, this is yet to be experimentally demonstrated. Therefore, the present study investigates the tool wear behavior in MAM turning of NGI with coated carbide tools. The results show that MAM can drastically reduce tool wear in turning NGI compared to CM. The effects of modulation frequency and amplitude on the tool wear are also evaluated. The wear reduction mechanism is also revealed and discussed.

2. Materials and methods

Figure 1 shows the setup used for carrying out both MAM and CM turning experiments. An in-house built piezo actuated modulation device was installed on a Haas TL-1 toolroom lathe to enable tool vibration in the feed direction during the turning process. The vibration frequency and amplitude were controlled by controlling a driving voltage applied to the piezo stack actuator of the modulation device. A detailed description of the modulation device can be found in Ref. [14].

The workpiece was a Dura-Bar ductile iron bar. Table 1 shows the chemical composition of the material. The material conforms to ASTM A536 grade 80-55-06 with a minimum tensile strength of 550 MPa. The nodular graphite was of Types I and II as defined in the ASTM A247 standard. The round bar workpiece had an initial diameter of 152.4 mm and a length of 254 mm. It was pre-machined to a diameter of 140 mm to remove the chill zone near the as-cast surface. Figure 2 shows the optical images of the microstructure of the material. The graphite nodules are surrounded by ferrite and contained in a matrix of pearlite. Based on the image analysis, the area percentage occupied by pearlite, ferrite, and graphite is 67.1%, 23.2%, and 9.7%, respectively.

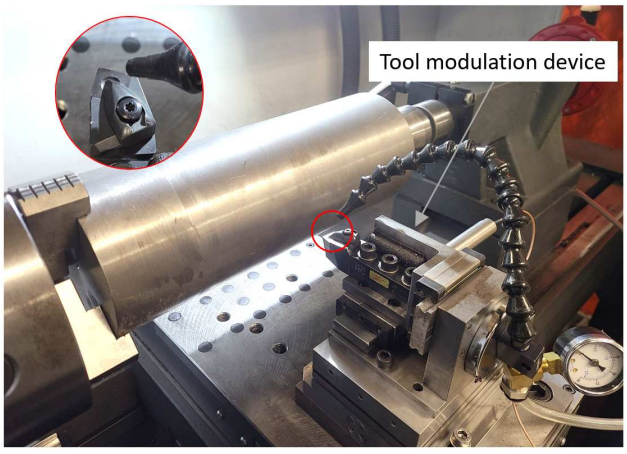

Figure 1: MAM turning setup.

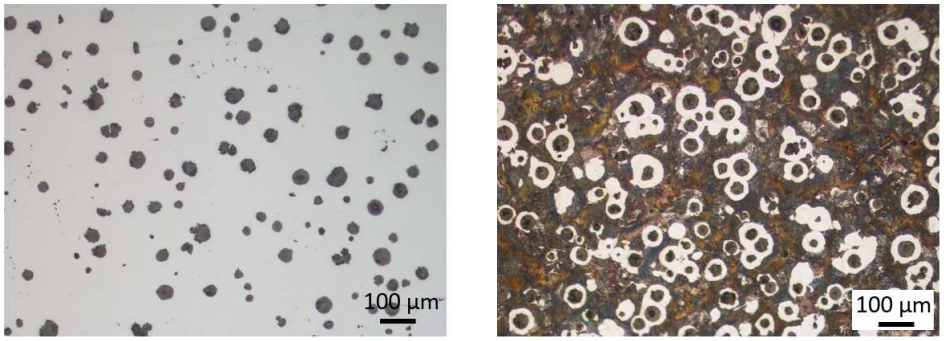

Figure 2: Microstructure of the NGI workpiece, a) unetched, b) etched with 3% Nital.

The cutting tool was a multi-layer coated carbide insert (Sandvik Coromant SNMA 12 04 08-KR 3205) which has TiCN and Al_2O_3 coatings on the rake face and TiCN + Al_2O_3 + TiN coatings on the flank face. The insert was used with Sandvik DSBNR 2020K tool holder. The resulting side cutting edge angle was 15°and the rake angle was -6°. The cutting fluid used in wet condition was Coolube 2210 (UNIST). The fluid was applied through a nozzle directed at the cutting zone from the rake face side (see inset in Fig. 1). The flow rate was about 1.7 ml/s.

Table 2 lists all the turning tests conducted in this study. Each test was conducted with a new tool. The baseline cutting parameters for both CM and MAM were kept the same for all tests, i.e., the cutting speed (v_c) was 350 m/min, the feed rate (h_0) was 0.04 mm/rev, and the depth of cut was 1.5 mm. The MAM parameters to be varied were the frequency ratio (f_m/f_w, ratio of modulation frequency to workpiece rotation frequency) and the modulation amplitude (A_{pp}, peak-to-peak). The modulation amplitude was mainly controlled by the driving voltage amplitude (V_{pp}). A_{pp} was measured to be 56 μm, 77 μm, and 91 μm for V_{pp} = 90 V, 120 V, and 150 V, respectively. However, the actual A_{pp} during cutting was reduced due to the elastic deformation of the modulation device assembly under the variable loading [15]. Based on the measured device stiffness and feed forces, the actual A_{pp} during cutting was estimated at about 40 μm, 55 μm, and 62 μm for V_{pp} = 90 V, 120 V, and 150 V, respectively.

The conducted tests involve four general types of cutting conditions which are illustrated in Fig. 3. The frequency ratio of integer values (i.e. $f_m/f_w = 4.0$) leads to MAM in-phase cutting (Fig. 3b), where the phase shift (ϕ) between two successive wavy tool paths is zero. In this case, cutting is still continuous with constant uncut chip thickness. The frequency ratio of half integer values (i.e., $f_m/f_w = 0.5$, 1.5, 3.5, 5.5, and 7.5) leads to MAM out-of-phase cutting (Fig. 3c and d), where $\phi = \pi$. During out-of-phase cutting with V_{pp} = 90 V, the modulation amplitude is not high enough to achieve tool-work disengagements (Fig. 3c). With V_{pp} = 120 V and 150 V, the modulation amplitude is sufficient

Table 2
List of turning tests and conditions.

Tool no.	Turning condition	Cutting distance (m)	$\frac{f_m}{f_w}$	V_{pp} (V)
1	CM-dry	600	-	-
2	CM-dry	1200	-	-
3	CM-dry	2000	-	-
4	MAM-dry	600	3.5	150
5	MAM-dry	1200	3.5	150
6	MAM-dry	2000	3.5	150
7	CM-wet	1200	-	-
8	MAM-wet	1200	3.5	150
9	MAM-dry	1200	4.0	150
10	MAM-dry	1200	0.5	150
11	MAM-dry	1200	1.5	150
12	MAM-dry	1200	5.5	150
13	MAM-dry	1200	7.5	150
14	MAM-dry	1200	3.5	120
15	MAM-dry	2000	3.5	120
16	MAM-dry	1200	3.5	90

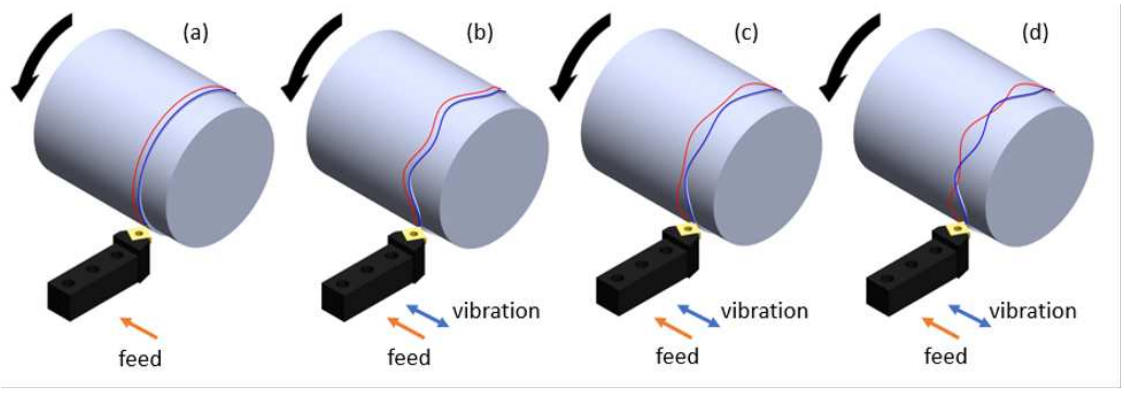

Figure 3: Schematic of a) CM, b) MAM in-phase cutting, c) MAM out-of-phase cutting without disengagements, and d) MAM out-of-phase cutting with disengagements.

to achieve tool-work disengagements during cutting (Fig. 3d). In the latter case, the increase in the integer part of the frequency ratio leads to the increase in the tool disengaging times per workpiece revolution. Detailed analysis of the cutting kinematics of MAM can be found in Ref. [11].

Before characterizing tool wear, the tool was cleaned by submerging it in an ethanol bath and then subjecting it to an ultrasonic cleaner. A Keyence VHX6000 digital microscope was used to measure tool wear. This digital microscope can also measure the 3D topography of the flank wear land. A JEOL 6610LV scanning electron microscope (SEM) with energy dispersive spectroscopy (EDS) was used to identify and measure the chemical compositions of the materials present on the tool. When significant adhesion occurred on the tool, the adhesion was removed by etching the tool with 19% hydrochloric acid (HCl) for 45 minutes. In this case, the above measurements were performed both before and after the etching.

3. Results

3.1. CM and MAM in dry condition

Figure 4 shows the flank wear curves for CM and MAM in dry condition. Tool wear was drastically reduced in MAM compared to CM. In CM, the flank wear (VB_{max}) progressed rapidly, increasing from 150 μm to 338 μm as the

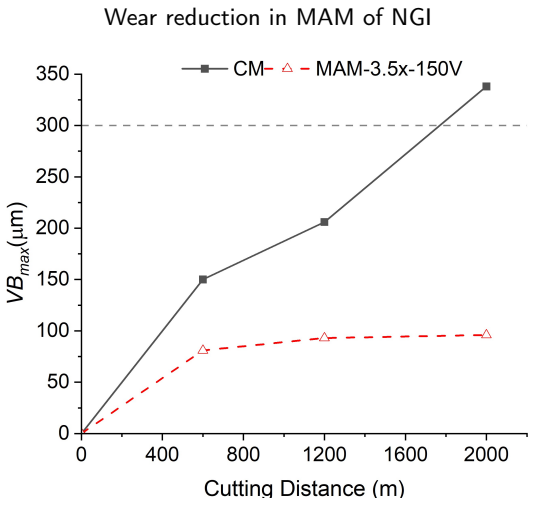

Figure 4: Progression of flank wear with cutting distance in CM and MAM in dry condition.

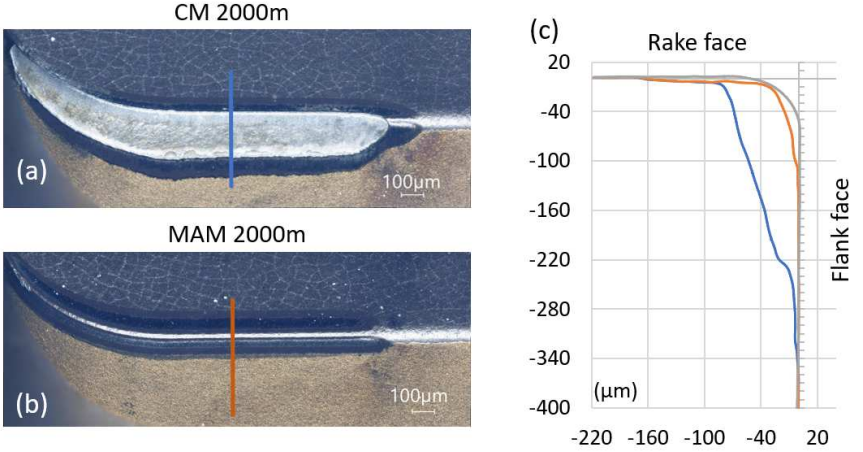

Figure 5: Digital images (a, b) and corresponding section profiles (c) of the main cutting edge for the tools after cutting 2000 m in CM and MAM in dry condition.

cutting distance was increased from 600 m to 2000 m. In MAM, except for the initial rapid wear, while establishing geometric conformity at the tool contact, the flank wear progressed very slowly. It only increased from 80 μm to 100 μm as the cutting distance was increased from 600 m to 2000 m. The wear curve remained nearly unchanged indicating a remarkably low wear rate. At the cutting distance of 2000 m, the flank wear was reduced by more than 70% in MAM compared to CM.

Figure 5 shows the images and the section profiles of the side cutting edge for the etched tools after cutting 2000 m. The section profile for CM (blue) shows not only the large flank wear width (measured along the flank face, i.e., VB) but also the large depth of the flank wear (measured normal to flank face). The flank wear depth was so large that the cutting edge was essentially destroyed (Fig. 5a). In contrast, the section profile for MAM (orange) shows both the width and depth of the flank wear were much smaller. The cutting edge geometry was not significantly altered and remained in good condition (Fig. 5b). Besides flank wear, the wear on the rake face can also be observed on the measured profile, which was quite small for both CM and MAM. Therefore, the flank wear is the dominant wear mode determining tool life in cutting NGI. The total wear volume in each case can be estimated by comparing the section profiles for CM and MAM with the profile for a new tool (gray). The wear volume is reduced by nearly 90% in MAM compared to CM.

Figure 6 shows the images of the flank face of the tool in CM at three cutting distances. In these images, the coating materials can be recognized by color (which was confirmed by EDS analysis): TiN appears golden, Al_2O_3 appears

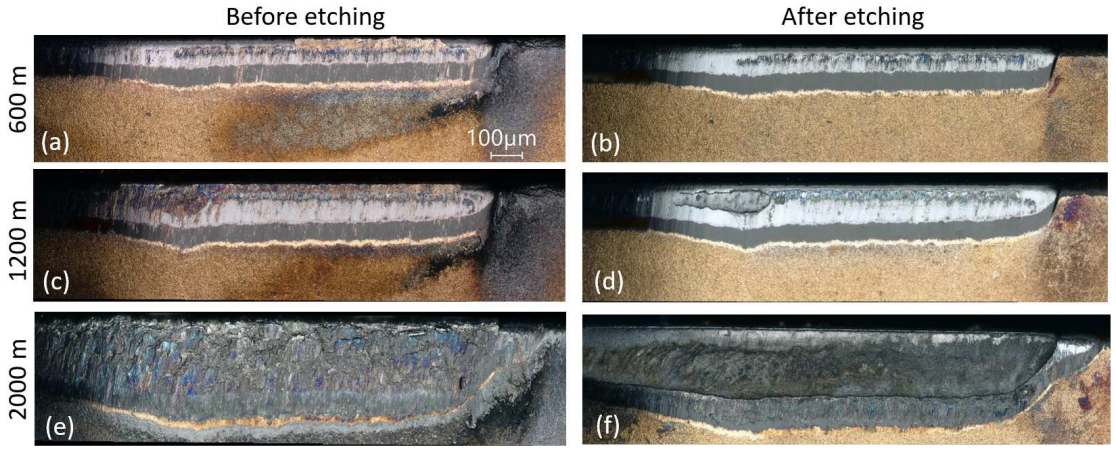

Figure 6: Digital images of the flank face of the tool at three cutting distances in dry CM.

dark gray, and TiCN appears white. After cutting 600 m, the wear front reached but did not breach the TiCN coating. Noticeably iron adhesion was accumulated along the cutting edge and the exposed TiCN coating near the trailing edge of the iron was discolored. While the iron was completely removed by etching, the discolored region on the exposed TiCN coating remained after etching. After cutting 1200 m, similar observations could be made on the iron adhesion along the cutting edge and the discolored region on exposed TiCN coating. Moreover, the wear front breached the TiCN coating and exposed the carbide near the nose side of the main flank. Iron adhesion occurred significantly on the exposed carbide region. After cutting 2000 m, severe iron adhesion occurred on almost the entire flank wear land as the carbide substrate was largely exposed. The wear progressed quite deep into the carbide as reflected by the section profile in Fig. 5c. The amount of iron adhesion was substantial. Even after 45-min etching, there was still a significant amount of iron left covering the carbide.

Figure 7 shows the images of the flank face of the tool in MAM at three cutting distances. The appearance of the tools before and after etching was drastically different. The images taken after etching clearly show the small flank wear land, which did not increase in size with increasing cutting distance. The noticeable change on the wear land was the exposed coating layers. After cutting 600 m, only Al_2O_3 coating (gray) was exposed; the wear did not reach TiCN coating. After cutting 1200 m, Al_2O_3 coating started to be breached near the cutting edge where TiCN coating was exposed. After cutting 2000 m, the exposed TiCN coating was appearing uniformly at the upper portion of the wear land, but there was no breaching of TiCN coating, so no carbide was exposed. The images taken before etching show a large amount of iron adhesion covering the entire length of the wear land after cutting 600 m and 1200 m, even though no carbide was exposed. After cutting 2000 m, the iron adhesion disappeared, but there appeared to be significant material depositions on the flank face as evidenced by the discoloration of the flank face.

Figure 8 shows the SEM images and EDS analysis of the flank face of the tool after cutting 1200 m in CM (the same tool as in Fig. 6c and d). The iron adhesion, tool coating layers, and exposed carbide were confirmed by the EDS analysis (spectra 1 – 4). It can be observed that a large fraction of the iron adhesion that appeared on the cutting edge in Fig. 6c disappeared in Fig. 8a. This was caused by ultrasonic cleaning of the tool before taking the SEM images. This suggests that the iron accumulated on the cutting edge was only weakly bonded to the tool. In contrast, the iron accumulated in the carbide-exposed flank region could not be removed without etching. The iron adhesion was more strongly bonded to the carbide. The discolored region on exposed TiCN coating as observed in Fig. 6c and d can also be identified on SEM images. EDS analysis (spectrum 3) indicates the formation of titanium dioxide (TiO_2) in the discolored region. TiO_2 cannot be etched by HCl, so it remained even after etching. TiO_2 should be formed due to the oxidation of TiCN. Except for the discolored region and carbide-exposed region, the rest of the flank wear land was not substantially covered by materials other than a few isolated small traces of iron.

Figure 9 shows the SEM image and EDS analysis of the flank face of the tool after cutting 1200 m in MAM (the same tool as in Fig. 7c and d). When comparing Fig. 9a with Fig. 7c, it can be observed that some portions of the iron adhesion were detached from the tool in Fig. 9a. This was again caused by ultrasonic cleaning before taking

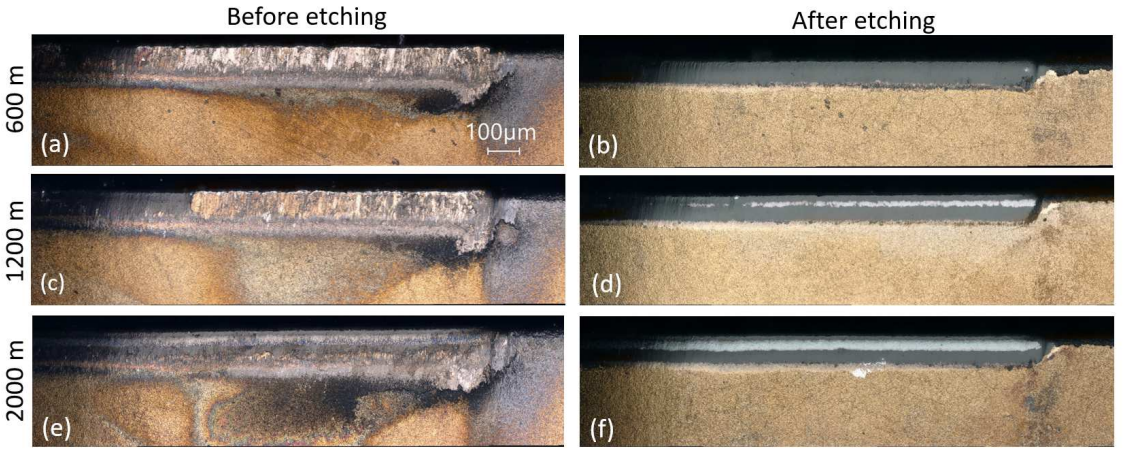

Figure 7: Digital images of the flank face of the tool at three cutting distances in dry MAM ($f_m/f_w = 3.5$, $V_{pp} = 150$ V).

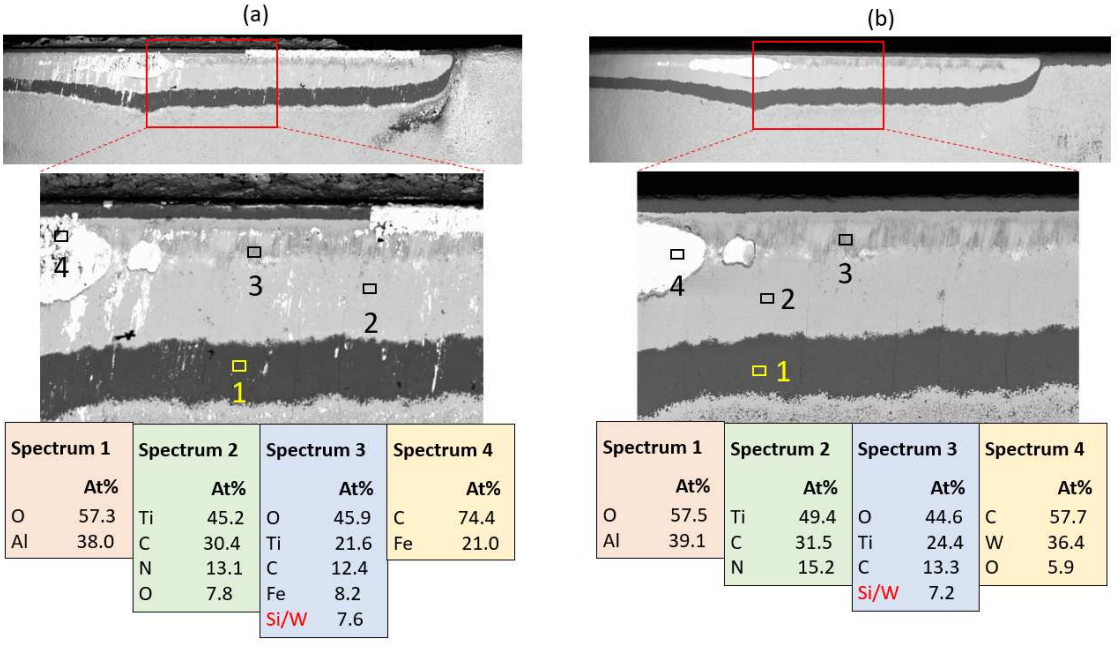

Figure 8: SEM images and EDS analysis of the flank face of the tool after cutting 1200 m in dry CM: a) before etching, b) after etching.

the SEM image, which indicates that the iron adhesion was weakly bonded to the tool. A closer examination of one iron-detached region (see Fig. 9b) reveals that there was an extra layer of material formed on the lower portion of the flank wear land. Based on the EDS analysis (see spectra 1 and 2 in Fig. 9b and elemental maps in Fig. 9c), the formed layer consisted of a large amount of magnesium oxide (MgO) and possibly a small amount of silicon dioxide (SiO_2). The Mg and Si elements should come from the work material. Their oxides were formed and deposited onto the tool flank face during cutting. Although Mg content was not reported by the material supplier in Table 1, it is well known that Mg needs to be added during casting NGI for creating the nodular graphite shape [16, 17]. The elemental maps of Mg and Si indicate that the distribution of the oxide layer was roughly uniform in the direction parallel to the cutting edge but had a gradient in the direction perpendicular to the cutting edge, i.e., the material flow direction. More oxides were deposited on the flank face as the work material moved away from the cutting edge. The thickest and densest oxide layer occurred just below the trailing edge of the flank wear land (on the unworn TiN coating). It can be also

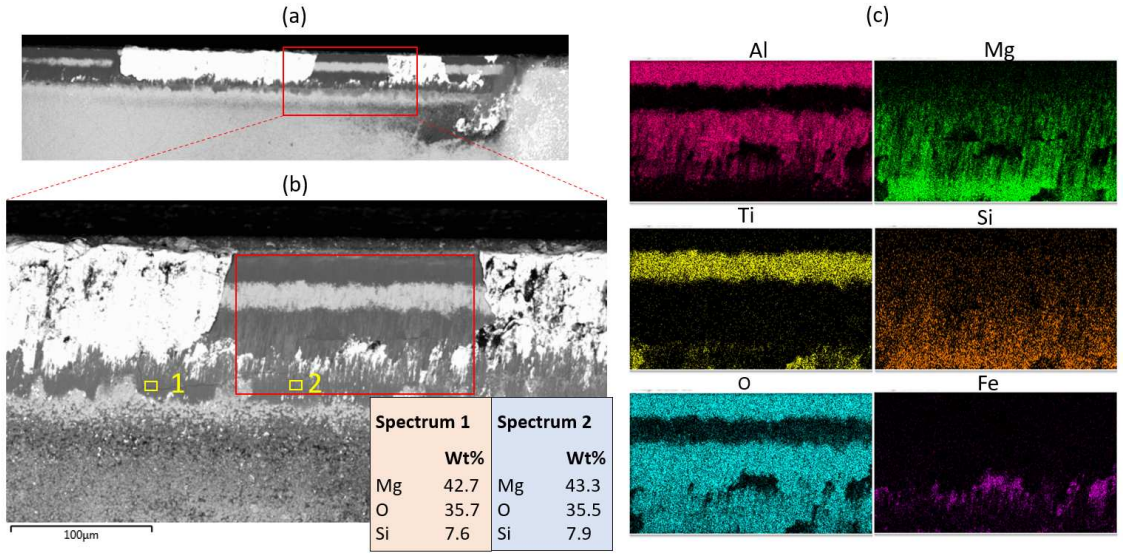

Figure 9: SEM image and EDS analysis of the flank face of the tool after cutting 1200 m in dry MAM, with (c) showing elemental maps of the rectangular region in (b).

observed in Fig. 9b that there were some residual iron spots left in the iron-detached region. This is also confirmed by the elemental map of Fe in Fig. 9c. This residual iron was roughly distributed along the line which marks the start of the thick and dense oxide layer near the trailing edge of the flank wear land. It seems that the main body of the iron layer which covered the most of flank wear land was merely bonded to and supported by the thick and dense oxide layer formed on the trailing edge of the flank wear land.

The oxide deposition layer together with the remaining iron adhesion could be completely removed by etching. EDS analysis of the etched tool showed no detection of any other materials except the tool coatings. This should confirm that the dominant oxide in the deposition layer was MgO as it is soluble in the HCl acid.

3.2. CM and MAM in wet condition

In addition to dry cutting, CM and MAM were also carried out in wet condition. Figure 10 shows the images of the flank face of the tools after cutting 1200 m in wet CM and MAM. Figure 11 shows the comparison of measured flank wear width (VB) between dry and wet cutting at the cutting distance of 1200 m. For CM, the application of cutting fluid did not significantly alter the wear behavior as compared to dry cutting (also see Fig. 6c and d). In wet CM, tool coating also started to be breached near the nose side of the main flank, and a large amount of iron adhesion occurred only in the carbide-exposed region. The rest of the wear land was generally clean with only small traces of iron. The only notable distinction from dry CM is that there was less discoloration of the TiCN coating in wet CM. The measured VB in wet CM was basically the same as in dry CM.

For MAM, the application of cutting fluid significantly changed the wear behavior and increased the flank wear as compared to dry cutting. Although the measured VB in wet MAM was much smaller than in wet CM, it was significantly larger than in dry MAM (Fig. 11). Unlike dry MAM, the iron adhesion in wet MAM did not cover continuously but occurred in regularly spaced patches on the flank wear land (Fig. 10c). After etching, the locations of these patches appeared as large pits or grooves oriented roughly perpendicular to the cutting edge. Correspondingly, the flank wear land had spiked in these locations, causing a larger difference between the average and maximum values of the measured VB in wet MAM (see Fig. 11).

Figure 12 shows the SEM image and EDS analysis of the flank face of the tool in wet MAM before etching (corresponding to Fig. 10c). It shows more clearly that iron adhesion was not continuously distributed but regularly spaced on the flank wear land. Furthermore, although MgO was detected on the coating region that was not covered by the iron adhesion (see spectra 2 and 3 and the elemental map of Mg), the MgO deposition was far less dense as compared to that in dry MAM (see Fig. 9).

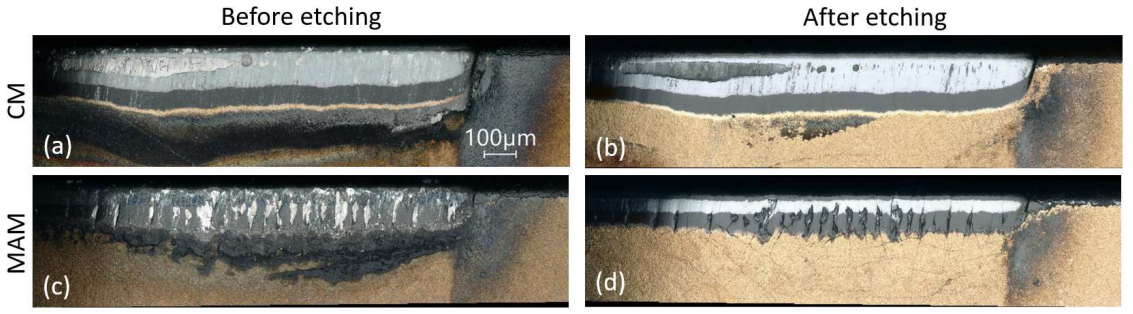

Figure 10: Digital images of the flank face of the tools after cutting 1200 m in wet CM and MAM.

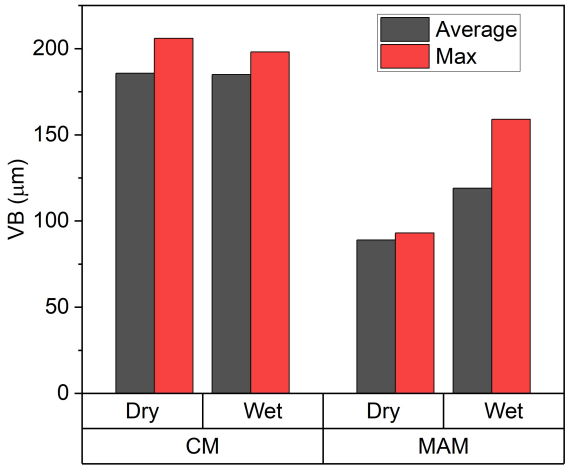

Figure 11: Comparison of flank wear (VB) between dry and wet cutting in CM and MAM (Cutting distance = 1200 m).

Figure 13 shows the SEM image and EDS analysis of the flank face of the tool in wet MAM after etching (corresponding to Fig. 10d). It can be observed that many cracks formed on the tool coatings. These were the thermal cracks caused by the larger temperature variation in wet MAM. Moreover, regularly spaced coating damages in the form of shallow pits occurred next to the cracks oriented approximately vertically. These shallow pits were the locations where iron adhesion occurred during cutting. EDS analysis shows these shallow pits only reached but did not breach the TiCN coating (see spectrum 1). The exposed TiCN coating inside these pits appeared much rougher than the exposed TiCN coating outside these pits. These shallow pits were likely formed from the thermal cracks. In wet MAM, the thermal cracks were large enough to trap iron within a small depth into these cracks during cutting. The iron was repeatedly trapped and removed causing attrition wear on the crack surfaces. This resulted in lateral expansion of the crack surfaces within a small depth, thereby creating shallow pits on the coatings.

3.3. Effect of modulation conditions

Since dry MAM resulted in better wear performance than wet MAM, further tests were carried out in dry MAM to investigate the effects of modulation conditions on the wear performance. Figure 14 shows the comparison of the measured flank wear (VB) for the tools after cutting the same distance (1200 m) at different modulation conditions. The result of dry CM is included as the baseline for the comparison. The test with $f_m/f_w = 4$ was MAM in-phase cutting ($\phi = 0$) where the cutting was continuous with constant uncut chip thickness like CM. As a result, the flank wear was as high as that in CM. The other tests were MAM out-of-phase cutting ($\phi = \pi$). The test with $V_{pp} = 90$ V had insufficient modulation amplitude where the tool was not fully disengaged during cutting. Therefore, it resulted in only a small wear reduction compared to CM. The tests with $V_{pp} = 120$ V and 150 V had sufficient modulation amplitude where tool-work disengagements were ensured during cutting. The resulting flank wear in these tests were all drastically lower

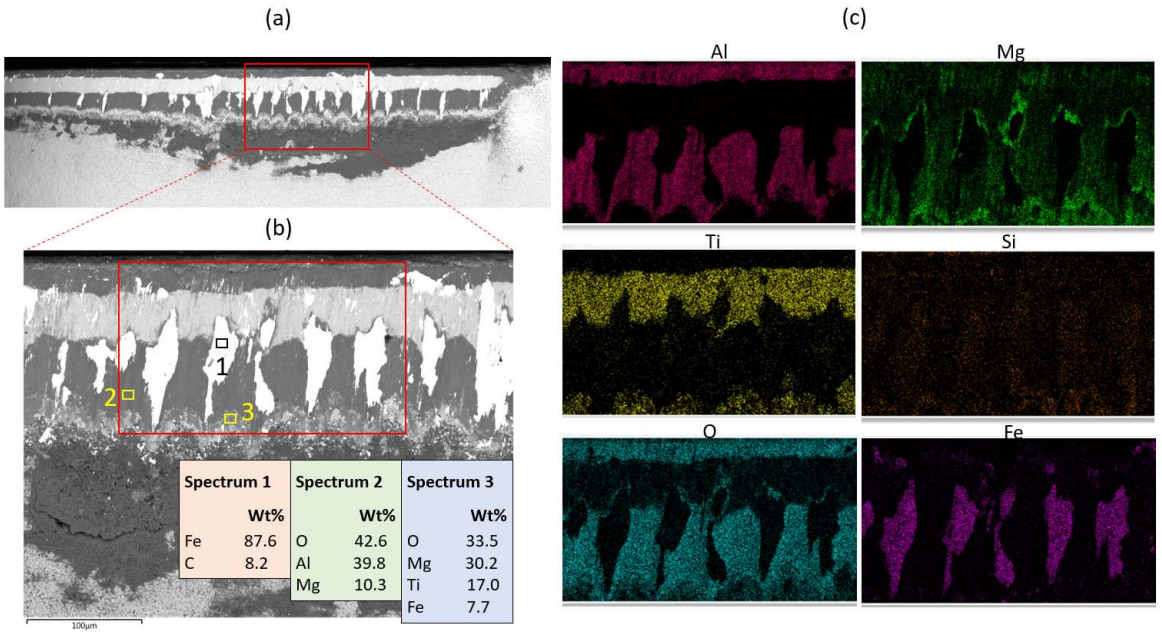

Figure 12: SEM images and EDS analysis of the flank face of the tool after cutting 1200 m in wet MAM, with (c) showing elemental maps of the rectangular region in (b).

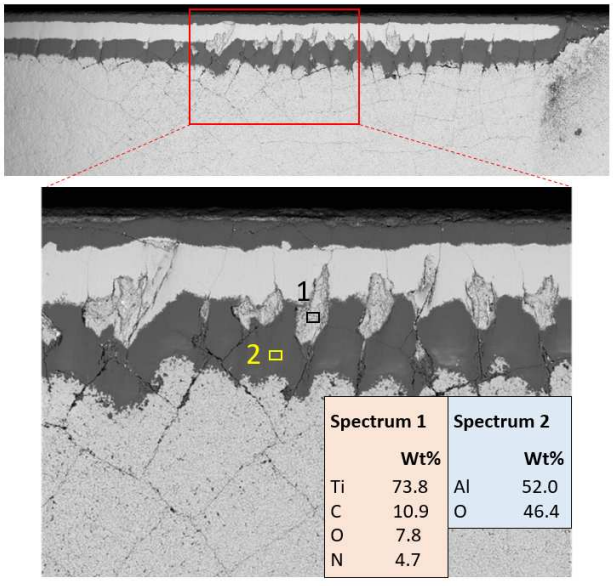

Figure 13: SEM images and EDS analysis of the flank face of the tool after cutting 1200 m in wet MAM after etching.

than that in CM. Therefore, achieving tool-work disengagements during cutting is the key condition for maximizing the wear reduction in MAM.

The tools used in MAM tests also showed two distinctive appearances corresponding to with or without tool-work disengagements during cutting. Figure 15 shows the images of the two tools without disengagement during cutting. Both tools had the same appearance as the tool used in CM (see Fig. 6). There was not much iron adhesion covering the flank wear land except along the cutting edge or in the carbide-exposed region. The exposed TiCN coating showed

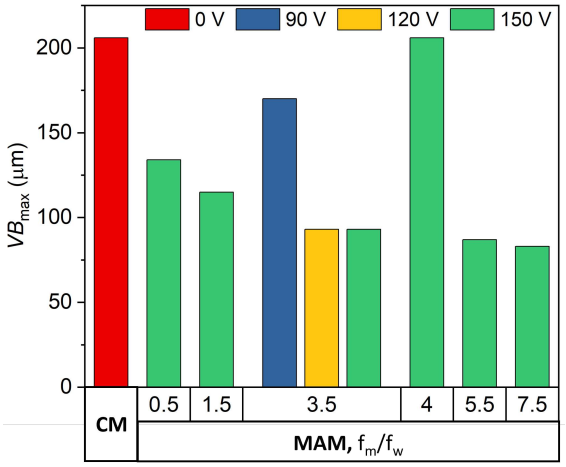

Figure 14: Comparison of the measured flank wear (VB) of tools after cutting 1200 m at different modulation conditions.

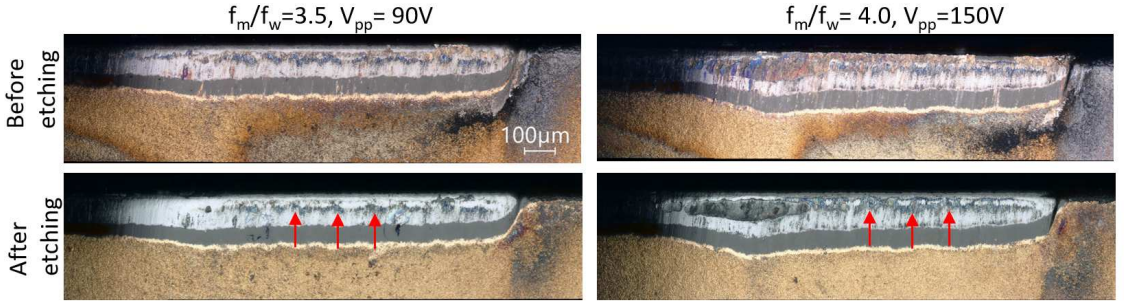

Figure 15: Digital images of the flank face of the tools after cutting 1200 m in dry MAM without tool-work disengagement during cutting.

discoloration due to its oxidation (see red arrows). Figure 16 shows the images of two tools with disengagements during cutting. They had the same appearance as the tool which was previously analyzed in Figs 7 and 9. Basically, there was a thick iron layer covering the flank wear land (see top row) which was only loosely attached to the tool as evidenced by its easy detachment from the tool by merely touching or ultrasonic cleaning (see middle row). There was also a dense and thick MgO layer formed near the trailing edge of the flank wear land (which was confirmed by EDS analysis). After etching, the flank wear land appeared very clean showing no discoloration of the exposed TiCN coating.

It was noted that the extent of flank wear (VB) was about the same for $V_{pp} = 120$ V and 150 V with a fixed frequency ratio (see $f_m/f_w = 3.5$ in Fig. 14 and compare Fig. 16f with Fig. 7f). This suggests that once tool-work disengagement is achieved, the wear will not be further reduced by further increasing the amplitude (i.e., increasing the disengagement duration). However, there was a noticeable decrease in wear with increasing the frequency ratio for MAM out-of-phase cutting ($\phi = \pi$) (see Fig. 14). The wear reduction by increasing frequency ratio was also observed on the rake face (Fig. 17). For $f_m/f_w = 0.5$, there was a large area of exposed TiCN in the wear region (in white color). The area of exposed TiCN became smaller as the frequency ratio increased. For $f_m/f_w = 7.5$, TiCN was no longer exposed along the main cutting edge. It was only exposed slightly along the minor cutting edge (around the tool nose).

4. Discussion

From the above results, there is no doubt that the wear of the coated carbide tools in turning NGI at high speed (350 m/min) can be drastically reduced (by multiple folds) by MAM compared to CM. On one hand, the drastic wear reduction occurs only when tool-work disengagements are achieved (through out-of-phase cutting with sufficient modulation amplitude) and cutting is performed in dry condition. On the other hand, the drastic wear reduction always

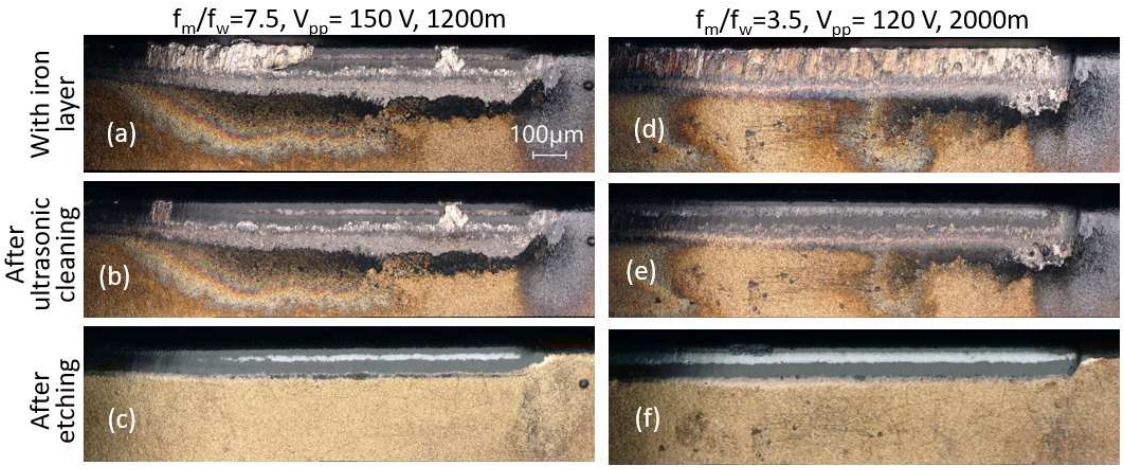

Figure 16: Digital images of the flank face of the tools in dry MAM with tool-work disengagements during cutting. (Top: tool with adhesion, middle: same tool without adhesion after cleaning, bottom: after etching)

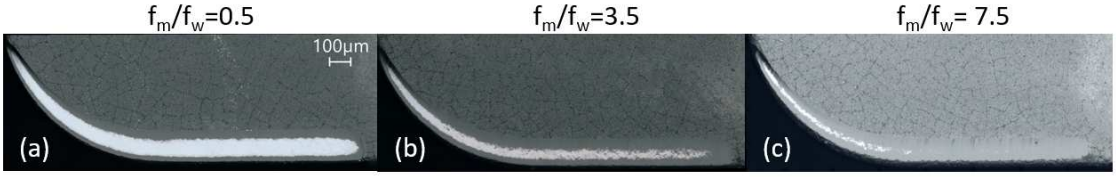

Figure 17: Digital images of tool rake face at three frequency ratios after 1200m cutting distance.

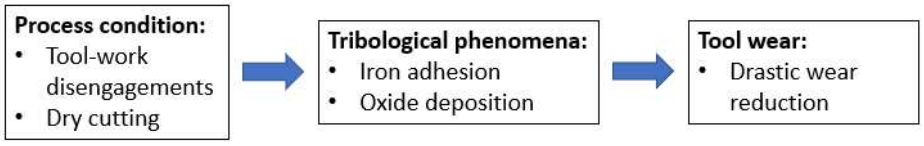

Figure 18: Summary of the relationship between MAM process conditions, tribological phenomena, and tool wear.

coincides with two observed tribological phenomena, i.e., iron adhesion and oxide (MgO) deposition at the tool flank face. Figure 18 summarizes the observed relationship among the process conditions, tribological phenomena, and tool wear. The tribological phenomena of iron adhesion and oxide deposition are the key to the understanding of the wear reduction mechanism in dry MAM, which will be further discussed.

4.1. Characteristics of the oxide layer and iron layer

Figure 19 illustrates the typical arrangement of the iron layer and oxide (MgO) deposition layer formed on the flank face. The MgO deposition occurs near the trailing edge of the flank wear land, which is accumulated as a dense and thick layer (blue box). This dense MgO layer is strongly attached to the tool coatings (as evidenced by its resistance to removal except by etching), and thus, is very stable. The iron layer occurs near the leading edge of the flank wear land which is above the dense MgO layer. This iron layer (red arrows) is not strongly bonded to the tool coatings as it can be easily removed by ultrasonic cleaning or gentle touching. Generally, iron does not adhere strongly to the tool coating materials, but it adheres strongly to the carbide [18]. This can also be inferred from the results of CM (see Fig. 6). The iron layer is formed due to the existence of the dense MgO deposition layer. The MgO deposition layer is thick enough to create geometrically a step or ramp (i.e., change in slope) on the flank face, which will slow down and even stop the iron flow on the flank face during cutting. The iron layer observed on the flank face is basically the stagnated iron that is left from the cutting. The iron layer is bonded to the tool not at its interface with the tool coatings (weak adhesion)

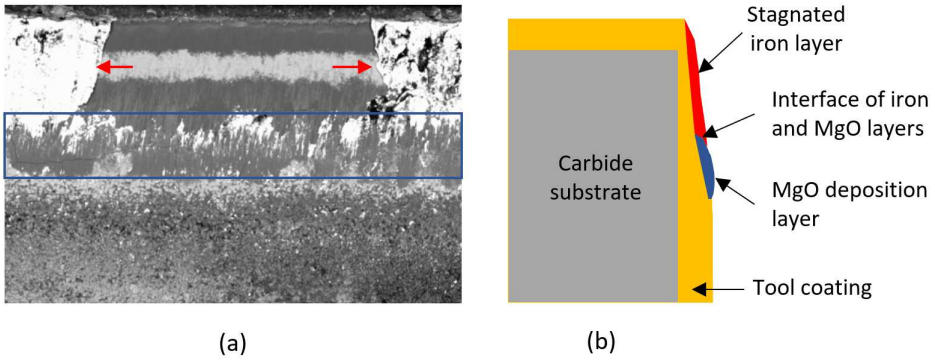

Figure 19: The arrangement of the iron and oxide layers on the flank face of the tool.

but at its interface with the MgO deposition layer (likely strong adhesion). Since only a small area of the iron layer is interfacing and bonded to the dense MgO layer, the main body of the iron layer is not stable and can be easily removed by ultrasonic cleaning or gentle touching.

4.2. Wear reduction mechanism

Both the MgO deposition layer and the stagnated iron layer serve as protective layers on the flank face during cutting. The MgO layer covering the trailing edge of the flank wear land is very stable. Once formed, it will not detach from the tool. During cutting, the MgO layer will be subjected to abrasion by the iron flow. However, its wear will be compensated by the continuous deposition of MgO at the same place. Therefore, the MgO layer will not wear out and the tool coating beneath the MgO layer will no longer be subjected to any abrasion from the iron flow.

The stagnated iron layer covering the leading edge of the flank wear land is not as stable as the MgO layer. During cutting, the stagnated iron layer will repeatedly detach and then re-form on the flank face. This, however, will not result in severe adhesion wear since the bonding between iron and the coating materials is very weak, but it will greatly reduce the speed of iron flow at the flank face (compared to the cutting speed). This will significantly reduce the rate of abrasive wear on the tool coatings.

In summary, the stable MgO layer stops the abrasive wear almost completely at the trailing edge of the flank wear land, while the stagnated iron layer significantly slows down the abrasive wear at the leading edge of the flank wear land. This explains the observed flank wear behavior in dry MAM (see Fig. 7b, d, and f). That is, with increasing cutting distance, there was only a slow increase in flank wear depth near the leading edge of the flank wear land (as evidenced by the exposed tool coating layers), but there was almost no increase in the flank wear land width (VB) due to the MgO layer at the trailing edge of the flank wear land.

The application of cutting fluid in MAM has two opposing effects. On one hand, it leads to better tool lubrication and cooling due to the periodic tool-work disengagements in MAM, which tends to reduce tool wear. On the other hand, it prevents the formation of the dense MgO deposition layer and stagnated iron layer on the tool flank face, thus negating the wear reduction attributed to protective layers. When comparing wet MAM with dry MAM, although the tool temperature is likely lower, the resulting tool wear is higher in wet MAM (see Fig. 11). This can be only explained by the lack of formation of the protective layers in wet MAM. This also indicates that the formation of these protective layers is more effective in reducing tool wear than the application of cutting fluid in MAM. In addition, the application of cutting fluid in MAM also creates large temperature variations and gradients on the tool which promote thermal cracks on tool coatings. The regularly spaced patches on the flank wear land in wet MAM are merely the coating damages originating from the thermal cracks. However, when comparing wet MAM with wet CM, although there are thermal cracks and related coating damages, the overall tool wear is still significantly lower in wet MAM (see Figs. 10 and 11). This wear reduction can be attributed to the enhanced tool lubrication and cooling effects in MAM (without the protective layer effect).

Even in dry cutting condition, the tool temperature is lower in MAM than in CM owing to the periodic tool-work disengagements. The more frequently the tool disengages from the workpiece during cutting, the lower is the tool temperature. This should explain the observed results that both the flank wear and crater wear decrease with increasing the frequency ratio in dry MAM (see Figs. 14 and 17). In dry MAM, the formation of protective layers on the tool flank

face is the primary mechanism for wear reduction; the temperature reduction due to tool-work disengagement can be considered as the secondary wear reduction mechanism.

4.3. Oxide layer formation

This wear reduction mechanism in MAM turning of NGI is very similar to that found previously in MAM turning of CGI [14]. However, the primary oxide deposition is SiO_2 when cutting CGI while it is MgO when cutting NGI. Both CGI and NGI contain a significant amount of Silicon (2-3 wt%) which promotes graphite formation. The Mg content is much smaller compared to the Si content. For CGI casting, Mg is added to consume sulfur and oxygen and produce vermicular-shaped graphite [19]. Mg content is generally higher in NGI than in CGI. For NGI casting, more Mg needs to be added to produce nodular-shaped graphite [16]. The free energy for the oxide formation is much lower for Mg than for Si [20]. Therefore, the oxide deposition layer changes from SiO_2 to MgO as the work material changes from CGI to NGI.

While different oxide layers may be formed depending on the work material, their formation seems to have a common mechanism that is dependent on the unique cutting kinematics of MAM. It has been shown that the oxide layer formation does not occur in CM, MAM in-phase cutting or MAM out-of-phase cutting with insufficient modulation amplitude. It only occurs when periodic tool-work disengagements are achieved in MAM (through out-of-phase cutting with sufficient amplitude). However, in the milling process, the cutting tool edges also disengage from the work material periodically, but there seems to be no such oxide layer formation in milling either NGI or CGI [21, 22]. This means that tool-work disengagement is a necessary but not a sufficient condition for the oxide layer formation.

Other necessary conditions may be inferred from the differences in the cutting kinematics between MAM and milling processes. One major difference is the tool disengaging time during each cutting cycle. In milling, the disengaging time is usually more than 50% of each tool revolution cycle [23]. In MAM, the tool is only disengaged for a very small fraction of each tool modulation cycle. This fraction is less than 15% in the present study. It may be the excessive cooling due to the longer disengaging time during each cutting cycle that prevents the formation of the oxide layer in milling. If so, the short disengaging time is a necessary condition for the oxide layer formation. Another difference is the variations of the effective rake angle and relief angle during cutting. In milling, both angles remain essentially constant at their nominal values. In MAM, these angles oscillate about their nominal values due to the tool modulation in the feed direction [24, 25]. In particular, the oscillation of the effective relief angle can lead to periodic variations in the contact pressure and contact area at the tool-work contact zone on the flank face. This may be important for the oxide layer formation. However, further study will be needed to test these hypotheses.

5. Conclusions

The tool wear behavior and wear reduction mechanism in MAM turning of nodular graphite iron (NGI) or ductile iron with coated carbide tool at high speed (350 m/min) has been experimentally studied. The main results of this study may be summarized as follows.

The flank wear is the primary form of wear during conventional (CM) turning of NGI. Under dry condition, the flank wear is substantially lower in MAM as compared to CM, with a reduction of over 70% in terms of flank wear land (VB) and nearly 90% in the volume removed due to flank wear.

The substantial wear reduction under dry MAM condition is primarily due to the formation of two protective layers on the flank face of the tool, i.e., the dense oxide (MgO) deposition layer formed near the trailing edge of the flank wear land, and the stagnated iron layer formed near the leading edge of the flank wear land. The formation of these layers only occurs in MAM when the tool is disengaged from the work material through out-of-phase cutting with sufficient modulation amplitude. In addition, tool wear can be further reduced by increasing the frequency ratio in MAM. However, further increasing modulation amplitude does not lead to more wear reduction.

Under wet condition, the flank wear is also significantly lower in MAM as compared to CM. Here the wear reduction is primarily due to better lubrication and cooling enhanced by periodic tool-work disengagements in MAM. However, because the cutting fluid prevents the formation of the protective layers on the flank face, the tool wear is higher in wet MAM than in dry MAM. In addition, MAM under wet condition promotes thermal cracks on the tool coatings, which can lead to coating damages. Therefore, MAM under dry condition should be preferred for cutting NGI with the coated carbide tool.

Acknowledgements

This work was supported by National Science Foundation CMMI grant no. 2019320.

References

[1] José Aécio G de Sousa, Wisley Falco Sales, and Alisson R Machado. A review on the machining of cast irons. *The International Journal of Advanced Manufacturing Technology*, 94:4073–4092, 2018.

[2] David A Stephenson and John S Agapiou. *Metal cutting theory and practice*. CRC press, 2016.

[3] PA Dearnley. A metallurgical evaluation of tool wear and chip formation when machining pearlitic grey cast irons with dissimilar graphite morphologies. *Wear*, 101(1):33–68, 1985.

[4] Recep Yigit, Erdal Celik, Fehim Findik, and Sakip Koksal. Effect of cutting speed on the performance of coated and uncoated cutting tools in turning nodular cast iron. *Journal of materials processing technology*, 204(1-3):80–88, 2008.

[5] Sirisak Tooptong, Kyung-Hee Park, and Patrick Kwon. A comparative investigation on flank wear when turning three cast irons. *Tribology International*, 120:127–139, 4 2018.

[6] W Grzesik and J Małecka. Documentation of tool wear progress in the machining of nodular ductile iron with silicon nitride-based ceramic tools. *CIRP annals*, 60(1):121–124, 2011.

[7] N. Camuşcu. Effect of cutting speed on the performance of Al_2O_3 based ceramic tools in turning nodular cast iron. *Materials* and *Design*, 27:997–1006, 1 2006.

[8] W Grzesik, P Kiszka, D Kowalczyk, J Rech, and Ch Claudin. Machining of nodular cast iron (pf-nci) using cbn tools. *Procedia CIRP*, 1:483–487, 2012.

[9] Varun Nayyar, Jacek Kaminski, Anders Kinnander, and Lars Nyborg. An experimental investigation of machinability of graphitic cast iron grades; flake, compacted and spheroidal graphite iron in continuous machining operations. *Procedia CIRP*, 1:488–493, 1 2012.

[10] Alborz Shokrani, Vimal Dhokia, and Stephen T Newman. Environmentally conscious machining of difficult-to-machine materials with regard to cutting fluids. *International Journal of machine Tools and manufacture*, 57:83–101, 2012.

[11] J. B. Mann, Y. Guo, C. Saldana, W. D. Compton, and S. Chandrasekar. Enhancing material removal processes using modulation-assisted machining. *Tribology International*, 44:1225–1235, 9 2011.

[12] Yang Guo, Tyler Stalbaum, James Mann, Ho Yeung, and Srinivasan Chandrasekar. Modulation-assisted high speed machining of compacted graphite iron (cgi). *Journal of Manufacturing Processes*, 15(4):426–431, 2013.

[13] Juan Sandoval, Aaqib Ali, Patrick Kwon, and Yang Guo. Modulation-assisted machining of compacted graphite iron with coated carbide tool in dry condition. *Manufacturing Letters*, 33:452–460, 9 2022.

[14] Juan Sandoval, Aaqib Ali, Patrick Kwon, David Stephenson, and Yang Guo. Wear reduction mechanisms in modulated turning of compacted graphite iron with coated carbide tool. *Tribology International*, 178:108062, 2 2023.

[15] Aaqib Ali, Jianxin Zhao, Patrick Kwon, Burak Sencer, and Yang Guo. Modulated orthogonal cutting system realized by piezo stack actuation and linear guide coupling. *Manufacturing Letters*, 35:468–476, 2023.

[16] Yoshio Igarashi and Senri Okada. Observation and analysis of the nucleus of spheroidal graphite in magnesium-treated ductile iron. *International Journal of Cast Metals Research*, 11(2):83–88, 1998.

[17] C Labrecque and M Gagne. Ductile iron: Fifty years of continuous development. *Canadian metallurgical quarterly*, 37(5):343–378, 1998.

[18] Israel Martinez, Ryutaro Tanaka, Yasuo Yamane, Katsuhiko Sekiya, Keiji Yamada, Tadahiro Ishihara, and Satoshi Furuya. Wear mechanism of coated tools in the turning of ductile cast iron having wide range of tensile strength. *Precision Engineering*, 47:46–53, 2017.

[19] Steve Dawson, I Hollinger, M Robbins, John Daeth, U Reuter, and H Schulz. The effect of metallurgical variables on the machinability of compacted graphite iron. *SAE transactions*, pages 334–352, 2001.

[20] James G. Speight. *Lange's Handbook of Chemistry*. McGraw-Hill Education, 2017.

[21] MB Da Silva, VTG Naves, JDB De Melo, CLF De Andrade, and WL Guesser. Analysis of wear of cemented carbide cutting tools during milling operation of gray iron and compacted graphite iron. *Wear*, 271(9-10):2426–2432, 2011.

[22] José AG de Sousa, Wisley Falco Sales, Wilson L Guesser, and Álisson R Machado. Machinability of rectangular bars of nodular cast iron produced by continuous casting. *The International Journal of Advanced Manufacturing Technology*, 98:2505–2517, 2018.

[23] Yusuf Altintas. *Manufacturing Automation: Metal Cutting Mechanics, Machine Tool Vibrations, and CNC Design*. Cambridge University Press, 2 edition, 2012.

[24] Zhang Deyuan and Wang Lijiang. Investigation of chip in vibration drilling. *International Journal of Machine Tools and Manufacture*, 38(3):165–176, 1998.

[25] Bora Eren and Burak Sencer. Mechanistic cutting force model and specific cutting energy prediction for modulation assisted machining. *Procedia Manufacturing*, 48:474–484, 2020.